In-situ micro-cantilever bending test in environmental scanning electron microscope: Real time observation of hydrogen enhanced cracking

Y. Deng, T. Hajilou, D. Wan, N. Kheradmand, A. Barnoush*

Department of Engineering Design and Materials, Norwegian University of Science and Technology, No-7491 Trondheim, Norway

A novel approach of in-situ micro-cantilever bending tests is introduced, integrating nanoindentation and environmental scanning electron microscopy (ESEM) to elucidate hydrogen embrittlement (HE) in FeAl. Bending tests were performed in vacuum (~5X10^{-4} Pa) and in ESEM with water vapor (180 Pa, 450 Pa) conditions, which introduce H in-situ into the cantilevers during the test. Micro-scale In-situ SEM testing provides a full control of all the parameters involved in HE as well as avoids the proximity effect from the free surface, which is always criticized in nano-scale in-situ TEM experiments. Both hydrogen induced cracking and hydrogen reduced flow stress were observed.

Keywords: in-situ test; iron aluminides (FeAl); hydrogen embrittlement;

Graphical abstract:

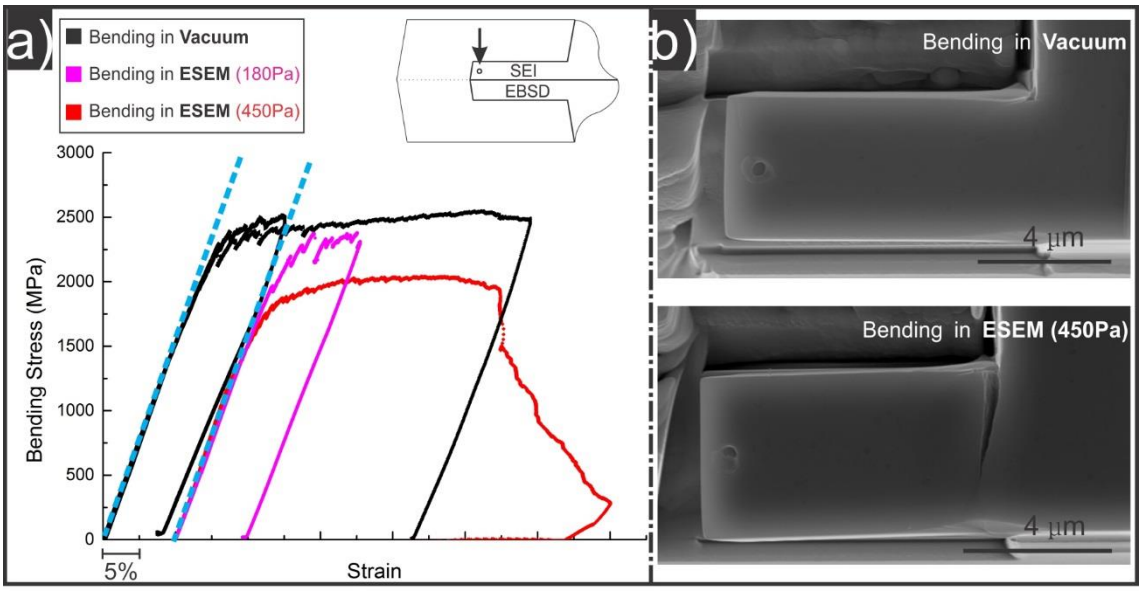

Hydrogen-enhanced or hydrogen-induced failure has been a topic of debate for the past decades. Different experimental observations and theoretical simulations proposed different models. One model is the hydrogen-enhanced decohesion (HEDE), which was proposed by Troiano in the 1960s [1], which simply postulated, that the hydrogen accumulated at the crack tip reduces the cohesive bond energy between atoms, thus decreasing the work needed for fracture to occur. The HEDE mechanism was found to agree with the observations that the crack tip opening angle decreases with rising hydrogen pressure in Fe-3Si (wt.%) and Ni single crystals [2]. Later, the HEDE mechanism has been expanded to the grain boundary and phase boundary area [3, 4] based on the experimental observations that hydrogen will weaken the boundary toughness, thus promoting intergranular fracture. The next proposed model is the hydrogen-enhanced localized plasticity (HELP), proposed mainly based on the in-situ observation of dislocation motion inside environmental TEM cells [5-8]. From these observations, the solid solution hydrogen increases the dislocation mobility or decreases the stacking fault energy, thus improving the cross-slip. These mechanisms will introduce local plasticity and strain softening, and thus explain the hydrogen-enhanced plastic failure. Another

alternative plasticity-based mechanism is the adsorption-induced dislocation emission (AIDE) reported in [9], which states that the formation energy of dislocations at crack tips is reduced by hydrogen adsorbed at the crack surface, after which crack propagation is prompted by dislocation motion. A recently proposed model, the defactant model, describes the HE based on the thermodynamic viewpoint [10, 11]. Analogous to the action of surfactants with surfaces, the segregation of H to defects (vacancies, dislocations, and boundaries) with an excess value of Γ will lower the defect formation energy.

Obviously, in order to experimentally depict and distinguish between these mechanisms, proper experimental setups are required to allow firstly in-situ charging H and secondly a full observation of H effect on the deformation process and microstructure evolution. We solved these challenges by the miniaturization of the experimental setup, where a full control on H charging, microstructural evolution as well as H affected zone is accessible.

In this paper, a novel approach was applied for bending micro-sized cantilevers in a setup with the combination of nanoindentation system and ESEM to meet the above mentioned requirements. Using a specimen scaling in micrometer size allows us to narrow down the parameters involved in HE under full control as well as to avoid the proximity effect from the free surface, which is always criticized in in-situ TEM experiments. The novelty of our approach is to utilize the ESEM as a hydrogen charging instrumentation. Given water vapor as the default environment in ESEM option, the test material is wisely chosen to the one that will be embrittled by moisture-produced hydrogen, i.e. the FeAl intermetallic alloy with B2 crystal-structure.

The detrimental effect of the environment on FeAl alloy was attributed to hydrogen embrittlement, where the atomic hydrogen was produced by the reaction of aluminum with water vapor [12-15]:

$$2\mathrm{Al}+3\mathrm{H_2O} \rightarrow \mathrm{Al_2O_3}+6\mathrm{H^+}+6\mathrm{e^-}$$

One can use the reaction kinetics to calculate the H concentration: $C_{[H]} = C_0$ [1- exp (-kt)] = $K_a K_r K_d P_{H2O}(C_{Al})^{1/3}$ [1- exp (-kt)], using K_a, K_r and K_d which are the rate constants for reactions of adsorption, oxidation, and dissolution of H, together with the P_{H2O} water partial pressure and C_{Al} the Al concentration in the alloy. Unfortunately, the available kinetic data for this are very limited and the experimental work to estimate them are lacking. Even though the hydrogen embrittlement of FeAl in a moisture-containing environment is widely agreed, the mechanism of hydrogen-assisted fracture is still not well understood. We explored the interaction of water vapor with FeAl alloy utilizing the novel approach proposed, and analyzed the HE effect further.

The single crystalline Fe-Al was grown by a modified Bridgeman technique [16]. Cantilevers were cut from this specimen, by a focused ion beam (Helios Nanolab DualBeam FIB, FEI Inc.) system with ~2×4×8 (μm) dimensions using 93 pA at 30 kV as the final current, in order to maintain a good surface quality. The cantilever beams have an initial orientation of $[4, \bar{3}, 23]$ parallel to normal direction and $[\overline{28}, 1, 5]$ parallel to loading direction, as shown in Fig. 1a. After ex-situ electron backscattered diffraction (EBSD) characterization, the beams were subjected to the load in-situ using the PI-85 Pico-indenter system (Hysitron Inc.) inside the ESEM (Quanta FEG 650 ESEM, FEI Inc.) in displacement-controlled mode with a 2.5 nm/s loading rate. The dwell time between loading and unloading steps was 20 s. Bending tests were performed both under vacuum (~5×10^{-4} Pa) and under water vapor (180 Pa, 450 Pa) conditions. The latter provides an in-situ H charging environment. *The beams were bent to 1 μm displacement in 180 Pa and to 5 μm displacement in 450 Pa ESEM conditions.* As shown in Fig. 1b, the cantilever is initially covered by a thin oxide layer created by the chemical reaction of aluminum with the moisture in air. During bending, small cracks will form on the oxide layer, which provide a pathway for water

molecules to contact with fresh FeAl matrix. The H produced by the chemical reaction of H_2O is transported to the tension area through diffusion. A minimum of three tests were conducted under each condition. The microstructure after bending was characterized using EBSD and TEM (JEM-2100, Jeol Inc.).

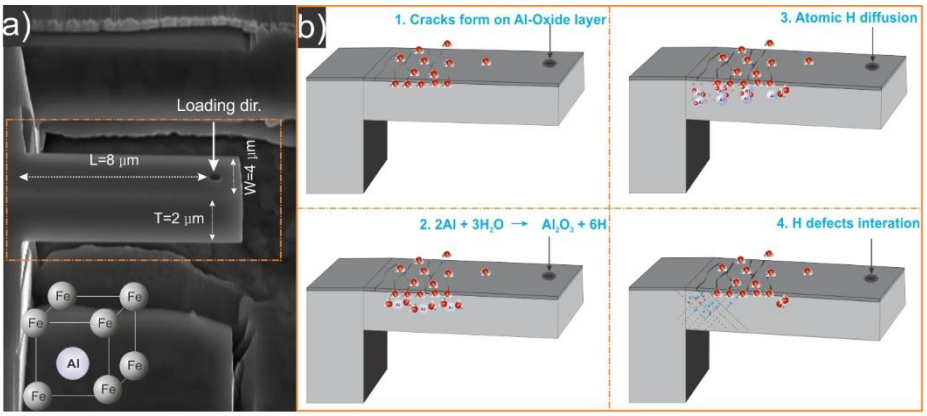

Fig.1 Side view of the FeAl single crystal cantilever after FIB milling before bending a); the principle of in-situ hydrogen charging within ESEM mode b).

The stress–strain curves shown in Fig. 2a were obtained from the force–displacement measurements. The bending stresses are calculated using Eq. (1), in which F, y, w, t refer to the forces, moment arms, width and thickness of the beams, respectively [17]. The corresponding strain, ϵ, was corrected by normalizing the displacement, d, with the moment arm, y. Due to the asymmetrical geometry of the beams, they were not bent around the same defined curvature radius, so the normalization of the displacements does not give the exact strains. However, the good agreement of the elastic stiffness among the different beams suggests that the moment arm is a reasonable normalization measure.

$$\sigma = \frac{4Fy}{w \cdot t^2} \tag{1}$$

Fig. 2 shows three different sets of experiments in which cantilevers were bent to 1 µm and 5 µm displacements under three different environmental conditions, i.e. in vacuum, in ESEM with 180 Pa and 450 Pa water vapor pressures. EBSD analysis was performed on the beams bent to 5 µm and TEM on the beams bent to 1 µm. For a better comparison, the flow curves tested in ESEM mode were offset by 0.1 unit on the strain axis.

The flow curves show a clear effect of the hydrogen from three main phenomena. 1) A reduction of yield strength (YS) was observed in ESEM mode. 2) The flow stresses (FS) of all the beams bent in water vapor environment decreased compared with those bent in vacuum. The reduction of FS increases with increasing water vapor pressure. 3) A continuous decrease of bending stress after 0.45 strain was detected, which is due to the propagation of cracks nucleated from the transition corner between the beam and bulk, as shown in Fig. $2c_1$.

The reduction of YS as one of the effects of hydrogen on FeAl has been pointed out previously in [18, 19]. In their experiments, the YS of Fe-40Al was found to decrease with decreasing strain rate when tested in air, while in vacuum the YS was independent of strain rate. One possible reason for the hydrogen-reduced YS is that hydrogen aids the heterogeneous nucleation of mobile dislocations at the surface. Reducing activation energy for homogeneous dislocation nucleation by hydrogen has been recently pointed out via in-situ electrochemical nanoindentation on FeAl single crystals [20]. After

further bending of the beam to 0.45 straining, cracks are nucleated from the triple corner of the cantilevers, where the beam experiences the highest tensile stress. Further propagation of the crack in a stable manner, the FS decreases continuously until the final 5 µm displacement is reached. The crack nucleation on the sample surface, when tested in air, has been observed previously in Fe-40Al alloy, while internal crack initiation was found when tested in O_2 atmosphere [21]. In our experiments no crack nucleation was observed in the tests performed in air (Fig.2b).

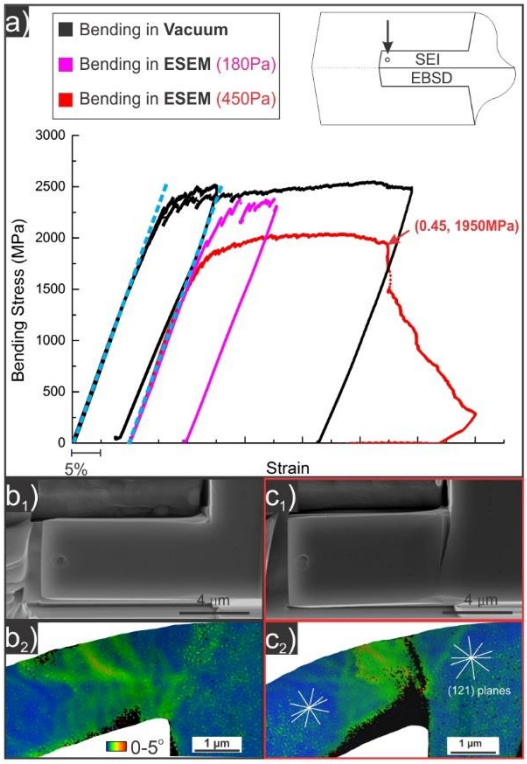

Fig. 2 Stress–strain curves a), Secondary Electron Imaging (SEI) and EBSD characterization together with the corresponding KAM analyses from the side cross section of the beams bent in vacuum b_1) b_2), and in ESEM c_1) c_2). The inset shows the the locations from which SEI and EBSD were conducted.

The local misorientation gradients are shown by Kernel Average Misorientation (KAM) maps, which qualify the average misorientation of one EBSD point with respect to a defined set of neighbors (the 3rd neighbor shell is used here), as shown in Fig. $2b_2$ and $2c_2$. The confidence index (CI) is higher than 0.1 for all the points shown here and points with CI lower than 0.1 are simply colored in black. The low CI values for the bottom part of the cantilever in Fig. $2c_2$ were due to the out-of-plane bending induced by the crack propagation from the corner to the outmost surface, which makes this region deflected from the 70° plane for EBSD. Hence, in order to interpret the results, we compare only the reliable EBSD data from the upper parts of beams. The following features are found from the above KAM maps: 1) The distributions of the misorientation at the top and the bottom are not identical due to the asymmetrical geometry of the root of the beam. 2) The misorientation gradient is more homogeneously distributed for the beam bent in vacuum, while for that bent in ESEM a more localized misorientation gradient to the crack region is observed. 3) A wavier pattern is observed in the beam bent in vacuum, while in ESEM mode, the slip traces are found to be more along certain slip planes (except for the center area where the density of dislocation is too high to be analyzed).

Fig. 3 shows the microstructure of the beams bent to 1 µm displacement in vacuum condition (Fig. $3a_{1-2}$) and in ESEM condition (Fig. $3b_{1-2}$). The slip traces revealed from the top of the beams, together with

the slip traces showed on the side of the beam in KAM images (Fig. 2c_2), suggest that slip systems with slip planes of $\{121\}$ are activated. This is consistent with Schmid's law, showing that the slip systems of $\{121\}[111]$ having the highest Schmid factor value of 0.47 for the selected orientation of the cantilevers.

The density of the slip lines is noticeably higher and more homogenously distributed in the beam tested in vacuum than that tested in ESEM mode, again reflecting a more uniform deformation obtained in vacuum mode. TEM samples are prepared from the cross-section of the beams. The results are shown in Fig. 3a_2 and b_2 for beams bent in vacuum and ESEM mode, respectively. TEM analysis was conducted with $\langle 001 \rangle$ zone axis. The lattice parameter measured from the diffraction pattern for this alloy is 0.304 nm, which fits well the previous measurement of 0.291 nm by X-ray diffraction on a powder sample [22]. By simply comparing the two weak-beam dark-field images, a reduction of the plastic zone area is found in the sample deformed in ESEM mode, which shows the consistency with the previous EBSD analysis. Moreover, a higher local strain is observed on the top part of the cantilever, being enclosed by a yellow circle, which may act as the initial site for crack nucleation.

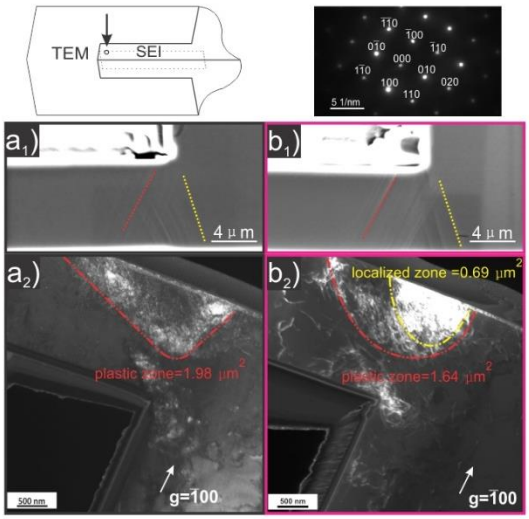

Fig. 3 Slip traces on the top of cantilevers deformed to 1 μm in a_1) vacuum and b_1) 180 Pa ESEM, and the weak-beam dark-field images from the cross-section of the beams a_2) and b_2).

The beam bent in ESEM mode was analyzed further under two different **g** vectors (**g**=$[\bar{1}00]$ and **g**=$[1\bar{1}0]$). Highly localized dislocation densities are found in the top and the bottom parts of the beam (Fig. 3a), indicating strong local strain concentrations. Most of the dislocations are visible under the **g**=$[\bar{1}00]$ vector but are invisible under the **g**= $[1\bar{1}0]$ vector, which shows that they have the Burgers vector of either $[111]$ or $[\bar{1}\bar{1}1]$. In addition to $\langle 111 \rangle$ type dislocations, some dislocations with a Burgers vector of $\langle 010 \rangle$ are shown in Fig. 4b, which are invisible under the **g**=$[\bar{1}00]$ vector and are visible under the **g**=$[1\bar{1}0]$ vector. The appearance of the $< 010 >$ type of dislocations has been observed previously in FeAl alloys after compression test. It was found that those dislocations were formed by the reaction of two $\langle 111 \rangle$ dislocations, and may act as a source for (001) cleavage fracture [23]. Further analysis needs to be done to understand the influence of hydrogen on the dislocation structure and the nucleation of the crack.

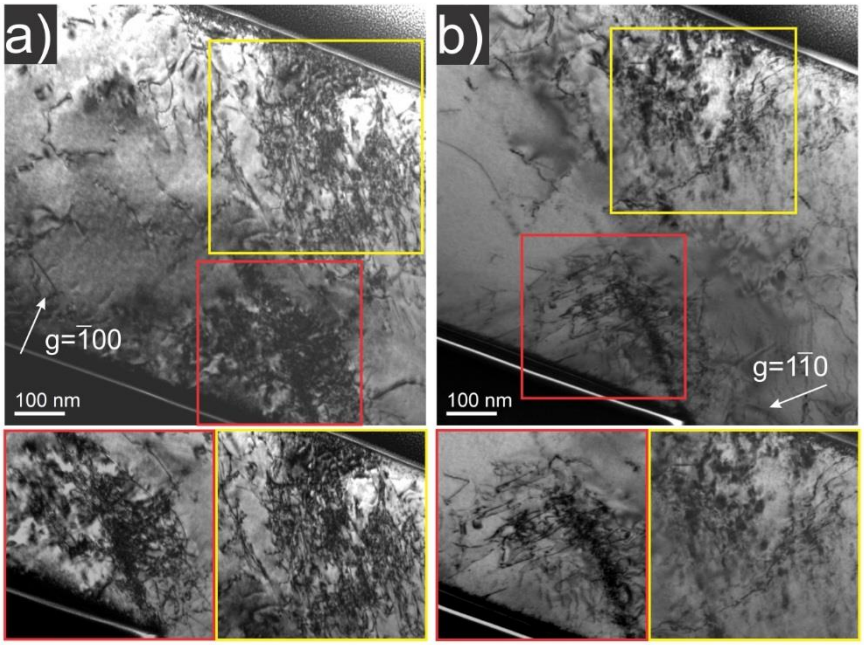

Fig. 4 Dark-field micrograph of cantilever bent with 180 Pa ESEM mode to 1 μm displacement in two **g**-vectors: a) **g**=[$\bar{1}$00] and b) **g**=[1$\bar{1}$0].

In our experiments of bending with H, we observed the reduced flow stress at the initial stage of bending, crack starting at the triple corner of the cantilever, and the localized plastic zone ahead of the crack. To author`s viewpoint, the HE works in following manner: 1) At low local H content, as expected to be present during the initial stage of the deformation and on the surface of the cantilevers, the H will reduce the nucleation energy of dislocations and double kinks, leading to a lower flow stress, as shown in Fig. 2a. 2) The highly stressed area, e.g. the triple corner on the cantilever, works as a notch and initiates the first crack in presence of the hydrogen, the high tensile stressed field at the crack tip will further attract H. This will enhance the dislocation nucleation from the crack tip, but at the same time reduce their mobility and shield the stress field by pinning. Therefore, the crack is growing in a brittle manner, and the observed macroscopic stress intensity factors is far below the H free condition [24]. This extremely localized plastic zone ahead of the crack tip can be seen in Fig. 2 C_2, where the black area on the upper part of the cantilever is due to the low indexing confidence in highly deformed zone. The idea of H reduced defects formation energy and H pinning have been proposed previously [25], however the exact H concentration that will cause pinning effect has not been clearly settled. In our experiment, the difficulty in quantifying the H concentration lays in the two following aspects: 1) the available kinetic data related to the adsorption, decomposition of the water vapor on the surface of aluminide intermetallic are very limited, which makes the calculation of H content from the kinetics equation difficult; 2) the interaction of electron beam with water molecules and surface, which will affect the fugacity of the water vapor, surface activity of the atoms [26]. New ideas need to be innovated with in-situ measuring H amount in this set-up.

In summary, a novel, clear in-situ setup integrating nanomechanical testing and ESEM is introduced, showing the ability to probe the effect of hydrogen in fully controllable mechanical and chemical conditions. The FeAl intermetallic alloy is tested in both vacuum and ESEM with water vapor conditions to elucidate the effect of moisture-produced hydrogen. From the mechanical point of view, the

hydrogen in FeAl reduces the YS, FS, and the strain to failure. The moisture-produced hydrogen reduces the plastic zone area and fac ilitates the nucleation of cracks on the sample surface. The prospect of this work is to localize H effect by introducing stress concentration on the locations of interest, e.g. by introducing notch on the cantilever surface to study the H effect further on mechanical properties of bulk, grain boundaries as well as phase boundaries.

Acknowledgements:

The Research Council of Norway is acknowledged for the support to the Norwegian Micro- and Nano-Fabrication Facility, NorFab. The TEM work was carried out on the NORTEM (JEM-2100), TEM Gemini Centre, Norwegian University of Science and Technology (NTNU), Norway. The authors also gratefully acknowledge the funding by HyF-Lex and HIPP projects.

[1] A.R. Troiano, R. Gibala, R. Hehemann, Hydrogen embrittlement and stress corrosion cracking: a Troiano Festschrift, ASM International1984.
[2] H. Vehoff, W. Rothe, Gaseous hydrogen embrittlement in FeSi- and Ni-single crystals, Acta Metallurgica 31(11) (1983) 1781-1793.
[3] Z. Tarzimoghadam, M. Rohwerder, S.V. Merzlikin, A. Bashir, L. Yedra, S. Eswara, D. Ponge, D. Raabe, Multi-scale and spatially resolved hydrogen mapping in a Ni–Nb model alloy reveals the role of the δ phase in hydrogen embrittlement of alloy 718, Acta Materialia 109 (2016) 69-81.
[4] M. Koyama, C.C. Tasan, E. Akiyama, K. Tsuzaki, D. Raabe, Hydrogen-assisted decohesion and localized plasticity in dual-phase steel, Acta Materialia 70 (2014) 174-187.
[5] S.D. House, J.J. Vajo, C. Ren, A.A. Rockett, I.M. Robertson, Effect of ball-milling duration and dehydrogenation on the morphology, microstructure and catalyst dispersion in Ni-catalyzed MgH2 hydrogen storage materials, Acta Materialia 86 (2015) 55-68.
[6] M.L. Martin, J.A. Fenske, G.S. Liu, P. Sofronis, I.M. Robertson, On the formation and nature of quasi-cleavage fracture surfaces in hydrogen embrittled steels, Acta Materialia 59(4) (2011) 1601-1606.
[7] A. Nagao, M.L. Martin, M. Dadfarnia, P. Sofronis, I.M. Robertson, The effect of nanosized (Ti,Mo)C precipitates on hydrogen embrittlement of tempered lath martensitic steel, Acta Materialia 74 (2014) 244-254.
[8] S. Wang, M.L. Martin, P. Sofronis, S. Ohnuki, N. Hashimoto, I.M. Robertson, Hydrogen-induced intergranular failure of iron, Acta Materialia 69 (2014) 275-282.
[9] S. Lynch, Hydrogen embrittlement phenomena and mechanisms, Corrosion Reviews 30(3-4) (2012).
[10] R. Kirchheim, Revisiting hydrogen embrittlement models and hydrogen-induced homogeneous nucleation of dislocations, Scripta Materialia 62(2) (2010) 67-70.
[11] R. Kirchheim, B. Somerday, P. Sofronis, Chemomechanical effects on the separation of interfaces occurring during fracture with emphasis on the hydrogen-iron and hydrogen-nickel system, Acta Materialia 99 (2015) 87-98.
[12] C.T. Liu, C.L. Fu, E.P. George, G.S. Painter, ENVIRONMENTAL EMBRITTLEMENT IN FEAL ALUMINIDES, Isij International 31(10) (1991) 1192-1200.
[13] C.T. Liu, E.P. George, P.J. Maziasz, J.H. Schneibel, Recent advances in B2 iron aluminide alloys: deformation, fracture and alloy design, Materials Science and Engineering a-Structural Materials Properties Microstructure and Processing 258(1-2) (1998) 84-98.
[14] L.M. Pike, C.T. Liu, Environmental and strain rate effects on the ductility and yield strength of Fe-40Al, Scripta Materialia 38(10) (1998) 1475-1480.
[15] L.M. Pike, C.T. Liu, The effect of vacancies on the environmental yield strength dependence of boron-free and boron-doped Fe-40Al, Intermetallics 8(12) (2000) 1413-1416.
[16] G. Bergmann, H. Vehoff, Precracking of NiAl single crystals by compression-compression fatigue and its application to fracture toughness testing, Scripta metallurgica et materialia 30(8) (1994) 969-974.

[17] E. Demir, D. Raabe, F. Roters, The mechanical size effect as a mean-field breakdown phenomenon: Example of microscale single crystal beam bending, Acta Materialia 58(5) (2010) 1876-1886.
[18] D. Wu, I. Baker, The effect of environment and strain rate on the room temperature tensile properties of FeAl single crystals, Intermetallics 9(1) (2001) 57-65.
[19] M. Chen, D. Lin, Y. Xia, C.T. Liu, Strain rate sensitivity of ductility and fracture behaviors in a Fe–28Al alloy, Materials Science and Engineering: A 239–240 (1997) 317-323.
[20] A. Barnoush, J. Dake, N. Kheradmand, H. Vehoff, Examination of hydrogen embrittlement in FeAl by means of in situ electrochemical micropillar compression and nanoindentation techniques, Intermetallics 18(7) (2010) 1385-1389.
[21] M.V. Nathal, C.T. Liu, Intrinsic ductility of FeAl single crystals, Intermetallics 3(1) (1995) 77-81.
[22] S.A. Makhlouf, T. Nakamura, M. Shiga, Structure and magnetic properties of FeAl1−xRhx alloys, Journal of Magnetism and Magnetic Materials 135(3) (1994) 257-264.
[23] P.R. Munroe, I. Baker, Observation of 〈001〉 dislocations and a mechanism for transgranular fracture on {001} in FeAl, Acta Metallurgica et Materialia 39(5) (1991) 1011-1017.
[24] P. Hirsch, S. Roberts, The brittle-ductile transition in silicon, Philosophical Magazine A 64(1) (1991) 55-80.
[25] M. Wen, S. Fukuyama, K. Yokogawa, Atomistic simulations of effect of hydrogen on kink-pair energetics of screw dislocations in bcc iron, Acta Materialia 51(6) (2003) 1767-1773.
[26] G.M. Bond, I.M. Robertson, H.K. Birnbaum, On the determination of the hydrogen fugacity in an environmental cell tem facility, Scripta Metallurgica 20(5) (1986) 653-658.